CASL
A DOE Energy Innovation Hub

CASL-U-2015-0176-000

Stability of S_N *K*-Eigenvalue Iterations using CMFD Acceleration

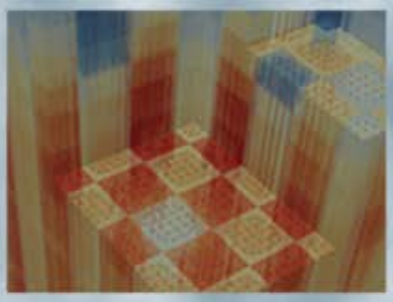

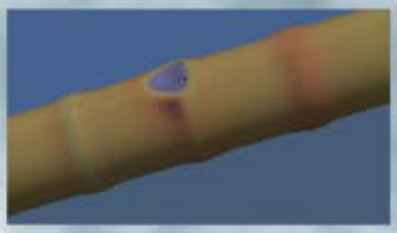

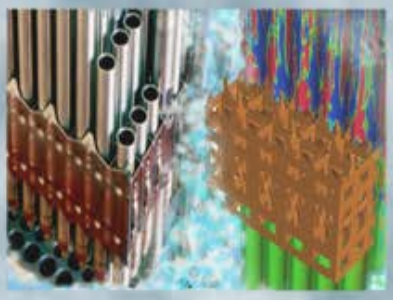

Kendra P. Keady and Edward W. Larsen
University of Michigan

April 19, 2015

U.S. DEPARTMENT OF ENERGY | Nuclear Energy

CASL-U-2015-0176-000

ANS MC2015 - Joint International Conference on Mathematics and Computation (M&C), Supercomputing in Nuclear Applications (SNA) and the Monte Carlo (MC) Method · Nashville, Tennessee · April 19–23, 2015, on CD-ROM, American Nuclear Society, LaGrange Park, IL (2015)

STABILITY OF S_N *K*-EIGENVALUE ITERATIONS USING CMFD ACCELERATION

Kendra P. Keady and Edward W. Larsen
Department of Nuclear Engineering and Radiological Sciences
University of Michigan
2355 Bonisteel Blvd, Ann Arbor, MI, 48105
keadyk@umich.edu; edlarsen@umich.edu

ABSTRACT

In this paper, a Fourier analysis is employed to assess the stability of discrete ordinates *k*-eigenvalue calculations with coarse-mesh finite difference (CMFD) acceleration using a fixed number of inner iterations per outer (hereafter referred to as the S_N-CMFD method). We describe the S_N-CMFD iteration equations for a representative one-dimensional *k*-eigenvalue transport problem. Since the *k*-eigenvalue iteration is inherently nonlinear, we linearize the system to produce equations amenable to Fourier analysis. This linearization is carried out for a homogeneous problem with periodic boundary conditions and an integer number of fine spatial cells per coarse cell. The subsequent Fourier analysis yields a matrix system of equations that can be solved to obtain the theoretical spectral radius. We compare the theoretical value to numerical estimates obtained using a 1-D S_N-CMFD simulation for a large slab problem with vacuum boundaries. The experimental values compare favorably with theoretical predictions for all cases considered. The Fourier analysis correctly predicts that the spectral radius decreases as M increases.

Key Words: Discrete ordinates, CMFD, Fourier analysis

1 INTRODUCTION

The CMFD method and its variants have been used to accelerate the convergence of many high-order deterministic calculations, using nodal, discrete-ordinates, and fine-mesh finite difference methods [1–3]. In the present work, we consider a common deterministic iteration scheme for *k*-eigenvalue calculations, consisting of the discrete ordinates method with step characteristic spatial differencing, CMFD acceleration, and a specified number of inner (scattering) sweeps per outer (fission source) iteration. We refer to this as the S_N-CMFD method. It is not well-understood how the convergence of the S_N-CMFD iteration scheme depends on the number of inner iterations performed per outer iteration, and other parameters in the problem (such as the coarse mesh thickness). Empirical evidence suggests that using more than one inner sweep per outer iteration reduces the spectral radius, but to our knowledge no attempt has been made to systematically study this effect theoretically.

Fourier analysis has been widely used to theoretically investigate the stability of deterministic methods for fixed-source problems [4], including nonlinear methods such as CMFD [5–7]. However,

to our knowledge, only two previous publications have used Fourier analysis to treat *k*-eigenvalue transport problems with CMFD acceleration. The first, by Hong, Kim, and Song [8], considers the discrete ordinates *k*-eigenvalue iteration with three different acceleration schemes, in addition to the unaccelerated case. Their analysis is restricted to problems with identical coarse/fine grids and a single inner iteration per outer. The second publication was written by the present authors, and considers the Monte Carlo-CMFD *k*-eigenvalue iteration in the limit as the number of Monte Carlo particles becomes infinite [9]. (The scattering source is treated implicitly in the Monte Carlo-CMFD Fourier analysis; this differs from the work presented here.) In the present paper, we use a Fourier analysis to study the stability of a *k*-eigenvalue problem with CMFD, and an arbitrary, fixed number of inner iterations per outer. We consider an arbitrary but specified number of fine spatial cells per coarse cell. This enables us to investigate the effect of coarse grid size on the stability of the method, while maintaining a realistic fine-grid optical thickness.

We show that the theoretical S_N-CMFD spectral radius (i) decreases as the scattering ratio increases (with the exception of the $M = 1$ case, which is discussed later), (ii) increases as the coarse grid size increases, and (iii) decreases as the number of inner iterations per outer increases. In the limit as the number of inner iterations per outer approaches infinity, the spectral radius limits to the implicit scattering result treated in [9]. These trends are discussed further in Section 5, where comparisons are made between theory and numerical experiment.

The remainder of this paper is organized as follows. In Section 2, we describe the equations that comprise the S_N-CMFD iteration scheme. In Section 3, we linearize the S_N-CMFD iteration equations, and in Section 4 we Fourier-analyze the linearized equations. In Section 5, we compare theoretical results from our Fourier analysis to numerical estimates from direct numerical simulations, and discuss these results. The paper concludes in Section 6 with a brief summary of our findings.

2 S_N ITERATION SCHEME WITH CMFD ACCELERATION

Here, we describe the iteration strategy for the S_N-CMFD method with a specified number of inner iterations per outer iteration. We consider a homogeneous slab geometry S_N *k*-eigenvalue transport problem on the domain $0 < x < X$, with isotropic scattering and periodic boundaries. We assume a fixed number (M) of inner scattering sweeps per outer fission source iteration, with m as the inner iteration index and l as the outer iteration index. With this notation, the l^{th} S_N iteration can be written as follows:

$$\phi_k^{(l+1/2,0)} = \phi_k^{(l)} \ , \ \ 1 \leq k \leq K \ , \tag{1a}$$

$$\frac{\mu_n}{h}(\psi_{k+1/2,n}^{(l+1/2,m)} - \psi_{k-1/2,n}^{(l+1/2,m)}) + \Sigma_t \psi_{k,n}^{(l+1/2,m)} = \frac{\Sigma_s}{2}\phi_k^{(l+1/2,m-1)} + \frac{\nu\Sigma_f}{2k^{(l)}}\phi_k^{(l)} \ , \tag{1b}$$

$$1 \leq n \leq N \ , \ \ 1 \leq k \leq K \ , \ \ 1 \leq m \leq M \ , \tag{1c}$$

$$\psi_{1/2,n}^{(l+1/2,m)} = \psi_{K+1/2,n}^{(l+1/2,m)} \ , \ \ 1 \leq n \leq N \ , \tag{1d}$$

$$\phi_k^{(l+1/2,m)} = \sum_{n=1}^{N} w_n \psi_{k,n}^{(l+1/2,m)} \ . \tag{1e}$$

The two terms on the right side of Eq. (1b) both contain scalar fluxes; however, these scalar fluxes represent different quantities. The scattering source flux ($\phi_k^{(l+1/2,m)}$) is updated at the conclusion of each inner iteration. The fission source flux ($\phi_k^{(l)}$) and eigenvalue ($k^{(l)}$) are held constant during inner iterations, and are later updated using the solution of the low-order CMFD system.

To close the high-order system of equations, we introduce the weighted diamond auxiliary equations:

$$\psi_{k,n}^{(l+1/2,m)} = \left(\frac{1+\alpha_n}{2}\right)\psi_{k+1/2,n}^{(l+1/2,m)} + \left(\frac{1-\alpha_n}{2}\right)\psi_{k-1/2,n}^{(l+1/2,m)} \ , \\ 1 \le n \le N \ , \ \ 1 \le k \le K \ . \tag{1f}$$

In this work, we use the *Step Characteristic* spatial discretization, with

$$\alpha_n = \frac{1+e^{-\Sigma_t h/\mu_n}}{1-e^{-\Sigma_t h/\mu_n}} - \frac{2\mu_n}{\Sigma_t h} \ , \ \ 1 \le n \le N \ . \tag{2}$$

Next, we impose a "coarse" grid on the problem domain, with J cells ($1 \le j \le J$) of width Δ. We also introduce the *coarse-grid parameter* p, which is defined as the number of fine cells per coarse cell:

$$p = \frac{\Delta}{h} \ . \tag{3}$$

After M scattering sweeps are performed, the solution of Eqs. (1) is used to calculate quantities defined on the coarse grid:

$$\Phi_j^{(l+1/2)} = \frac{1}{p}\sum_{k\in j}\phi_k^{(l+1/2,M)} \ , \tag{4a}$$

$$\Phi_{1,j\pm1/2}^{(l+1/2)} = \sum_{n=1}^{N} w_n\mu_n\psi_{j\pm1/2,n}^{(l+1/2,M)} \ . \tag{4b}$$

In general, the coarse-grid flux-weighted cross sections must also be calculated; however, they are known exactly for the homogeneous problem considered here. The interior-edge CMFD correction factors are calculated using

$$\hat{D}_{j+1/2}^{(l+1/2)} = \frac{\Phi_{1,j+1/2}^{(l+1/2)} + \frac{1}{3\Sigma_t\Delta}(\Phi_{j+1}^{(l+1/2)} - \Phi_j^{(l+1/2)})}{\Phi_{j+1}^{(l+1/2)} + \Phi_j^{(l+1/2)}} \ , \tag{4c}$$

while the exterior-edge values are obtained using the periodic boundary condition:

$$\hat{D}_{1/2}^{(l+1/2)} = \hat{D}_{J+1/2}^{(l+1/2)} = \frac{\Phi_{1,1/2}^{(l+1/2)} + \frac{1}{3\Sigma_t\Delta}(\Phi_1^{(l+1/2)} - \Phi_J^{(l+1/2)})}{\Phi_1^{(l+1/2)} + \Phi_J^{(l+1/2)}} \ . \tag{4d}$$

Here, capital letters (Φ, D, Δ) are used to denote coarse-grid quantities, while lower-case letters (ψ, ϕ, h) denote fine-grid quantities. After the coarse-grid quantities are calculated, we build and solve the following low-order CMFD system:

$$\Phi_{1,j+1/2}^{(l+1)} - \Phi_{1,j-1/2}^{(l+1)} + \Sigma_a \Phi_j^{(l+1)} \Delta = \frac{\nu \Sigma_f}{k^{(l+1)}} \Phi_j^{(l+1)} \Delta \ , \ \ 1 \leq j \leq J \ , \tag{5a}$$

$$\Phi_{1,j+1/2}^{(l+1)} = \frac{1}{3\Sigma_t \Delta} (\Phi_{j+1}^{(l+1)} - \Phi_j^{(l+1)}) + \hat{D}_{j+1/2}^{(l+1/2)} (\Phi_{j+1}^{(l+1)} + \Phi_j^{(l+1)}) \ , \tag{5b}$$

$$\Phi_{1,1/2}^{(l+1)} = \Phi_{1,J+1/2}^{(l+1)} \ , \tag{5c}$$

$$1 = \frac{1}{J} \sum_{j=1}^{J} \Phi_j^{(l+1)} \ . \tag{5d}$$

The low-order discrete Eqs. (5) are consistent with the continuous one-dimensional transport equation, and on convergence, their solution would yield the true scalar fluxes, volume-averaged over each coarse cell. The low-order system is not tridiagonal for the periodic boundary case treated in this work. To complete the iteration scheme, we introduce the "update" equation:

$$\phi_k^{(l+1)} = \phi_k^{(l+1/2,M)} \left[\frac{\Phi_j^{(l+1)}}{\Phi_j^{(l+1/2)}} \right] \ , \ \ k \in j \ , \ \ 1 \leq j \leq J \ . \tag{6}$$

Eq. (6) uses the solution of the low-order CMFD system to "scale" the fine-grid fission source for the next outer iteration. This expression preserves the shape of the fine-grid solution within each coarse cell, while adjusting the amplitude such that the fine-grid solution average over a coarse cell is consistent with the updated low-order solution.

To summarize, a single S_N-CMFD *k*-eigenvalue iteration consists of the following steps: (i) perform a fixed number (M) of high-order scattering sweeps, (ii) use the high-order quantities to calculate the CMFD system, (iii) solve the CMFD system to obtain an updated estimate of the fission source, and (iv) use the upated fission source to scale the fine-grid fission source for the next iteration.

The S_N-CMFD *k*-eigenvalue iteration scheme is inherently nonlinear. Next, we linearize Eqs. (1) - (6) to make the method amenable to Fourier analysis.

3 LINEARIZATION

To linearize the S_N-CMFD system, we consider the problem shown in Eqs. (1) - (6). On convergence, this problem has the exact solution

$$\psi_{k,n} = \psi_{k\pm 1/2,n} = \frac{1}{2} \ , \tag{7a}$$

$$\Phi_j = \phi_k = 1 \ , \tag{7b}$$

$$\Phi_{1,j+1/2} = 0 \ , \tag{7c}$$

$$k = \frac{\nu\Sigma_f}{\Sigma_a} \ . \tag{7d}$$

To proceed, we define the following linear expansions around the exact solution (with $\epsilon << 1$):

$$\psi_{k,n}^{(l+1/2,m)} = \frac{1}{2} + \epsilon\tilde{\psi}_{k,n}^{(l+1/2,m)} \ , \tag{8a}$$

$$\psi_{k\pm1/2,n}^{(l+1/2,m)} = \frac{1}{2} + \epsilon\tilde{\psi}_{k\pm1/2,n}^{(l+1/2,m)} \ , \tag{8b}$$

$$\phi_{k}^{(l+1/2,m)} = 1 + \epsilon\tilde{\phi}_{k}^{(l+1/2,m)} \ , \tag{8c}$$

$$\phi_{k}^{(l+1)} = 1 + \epsilon\tilde{\phi}_{k}^{(l+1)} \ , \tag{8d}$$

$$\Phi_{j}^{(l+1/2)} = 1 + \epsilon\tilde{\Phi}_{j}^{(l+1/2)} \ , \tag{8e}$$

$$\Phi_{j}^{(l+1)} = 1 + \epsilon\tilde{\Phi}_{j}^{(l+1)} \ , \tag{8f}$$

$$\Phi_{1,j+1/2}^{(l+1/2)} = 0 + \epsilon\tilde{\Phi}_{1,j+1/2}^{(l+1/2)} \ , \tag{8g}$$

$$\Phi_{1,j+1/2}^{(l+1)} = 0 + \epsilon\tilde{\Phi}_{1,j+1/2}^{(l+1)} \ , \tag{8h}$$

$$\hat{D}_{j+1/2}^{(l+1/2)} = 0 + \epsilon\hat{d}_{j+1/2}^{(l+1/2)} \ , \tag{8i}$$

$$\frac{1}{k^{(l+1)}} = \frac{\Sigma_a}{\nu\Sigma_f} + \epsilon\delta^{(l+1)} \ . \tag{8j}$$

The coarse-grid cross sections are known exactly for the homogeneous problem, so these quantities are not expanded. We insert Eqs. (8) into Eqs. (1) - (6). The $\mathcal{O}(1)$ terms cancel out, and we equate $\mathcal{O}(\epsilon)$ and ignore $\mathcal{O}(\epsilon^2)$ terms to obtain:

$$\tilde{\phi}_{k}^{(l+1/2,0)} = \tilde{\phi}_{k}^{(l)} \ , \ \ 1 \le k \le K \ , \tag{9a}$$

$$\frac{\mu_n}{h}(\tilde{\psi}_{k+1/2,n}^{(l+1/2,m)} - \tilde{\psi}_{k-1/2,n}^{(l+1/2,m)}) + \Sigma_t\tilde{\psi}_{k,n}^{(l+1/2,m)} = \frac{\Sigma_s}{2}\tilde{\phi}_{k}^{(l+1/2,m-1)} + \frac{\nu\Sigma_f}{2}\delta^{(l)} + \frac{\Sigma_a}{2}\tilde{\phi}_{k}^{(l)} \ , \tag{9b}$$

$$1 \le n \le N \ , \ \ 1 \le k \le K \ , \ \ 1 \le m \le M \ ,$$

$$\tilde{\psi}_{1/2,n}^{(l+1/2,m)} = \tilde{\psi}_{K+1/2,n}^{(l+1/2,m)} \ , \ \ 1 \le n \le N \ , \tag{9c}$$

$$\tilde{\phi}_{k}^{(l+1/2,m)} = \sum_{n=1}^{N} w_n\tilde{\psi}_{k,n}^{(l+1/2,m)} \ , \tag{9d}$$

$$\tilde{\Phi}_{j}^{(l+1/2)} = \frac{1}{p}\sum_{k\in j}\tilde{\phi}_{k}^{(l+1/2,M)} \ , \tag{9e}$$

$$\tilde{\Phi}_{1,j+1/2}^{(l+1/2)} = \sum_{n=1}^{N} w_n\mu_n\tilde{\psi}_{(jp)+1/2,n}^{(l+1/2,M)} \ , \tag{9f}$$

$$\hat{d}_{j+1/2}^{(l+1/2)} = \frac{1}{2}\left[\tilde{\Phi}_{1,j+1/2}^{(l+1/2)} + \frac{1}{3\Sigma_t\Delta}(\tilde{\Phi}_{j+1}^{(l+1/2)} - \tilde{\Phi}_{j}^{(l+1/2)})\right] \ , \tag{9g}$$

$$\frac{1}{\Delta}(\tilde{\Phi}_{1,j+1/2}^{(l+1)} - \tilde{\Phi}_{1,j-1/2}^{(l+1)}) = \nu\Sigma_f\delta^{(l+1)} \ , \tag{9h}$$

$$\tilde{\Phi}_{1,j+1/2}^{(l+1)} = -\frac{1}{3\Sigma_t\Delta}(\tilde{\Phi}_{j+1}^{(l+1)} - \tilde{\Phi}_j^{(l+1)}) + 2\hat{d}_{j+1/2}^{(l+1/2)} \ , \tag{9i}$$

$$0 = \frac{1}{J}\sum_{j=1}^{J} \tilde{\Phi}_j^{(l+1)} \ , \tag{9j}$$

and

$$\tilde{\phi}_k^{(l+1)} = \tilde{\phi}_k^{(l+1/2,M)} + \tilde{\Phi}_j^{(l+1)} - \tilde{\Phi}_j^{(l+1/2)} \ , \quad k \in j \ , \ \ 1 \leq j \leq J \ . \tag{9k}$$

We note that several of Eqs. (9) differ in form from Eqs. (1) - (6). This occurs because the original equations contain nonlinear terms. Summing Eq. (9h) over all coarse cells, we immediately obtain:

$$\delta^{(l+1)} = 0 \ . \tag{10}$$

Thus, the S_N-CMFD iteration scheme converges the $\mathcal{O}(\epsilon)$ component of the eigenvalue (but not the eigenfunction) after a single iteration. In the following section, we perform the Fourier analysis to estimate the rate at which the eigenfunction converges, as a function of the coarse grid optical thickness, scattering ratio, and number of inner iterations per outer.

4 FOURIER ANALYSIS

Before introducing the Fourier ansatz, we define a new, relative index to simplify the analysis:

$$k = (j-1)p + r \ . \tag{11}$$

In Eq. (11), k is the fine cell index, j is the index of the coarse cell in which fine cell k resides, p is the coarse-grid parameter (introduced in Section 2), and r is the position of fine cell k within coarse cell j. Using this new indexing system, the Fourier ansatz can be expressed:

$$\tilde{\psi}_{k-1/2,n}^{(l+1/2,m)} = \omega^l A_{r,n}^{(m)} e^{i\Sigma_t\lambda x_j} \ , \tag{12a}$$

$$\tilde{\psi}_{k,n}^{(l+1/2,m)} = \omega^l B_{r,n}^{(m)} e^{i\Sigma_t\lambda x_j} \ , \tag{12b}$$

$$\tilde{\phi}_k^{(l+1/2,m)} = \omega^l F_r^{(m)} e^{i\Sigma_t\lambda x_j} \ , \tag{12c}$$

$$\tilde{\Phi}_j^{(l+1/2)} = \omega^l D e^{i\Sigma_t\lambda x_j} \ , \tag{12d}$$

$$\tilde{\Phi}_{1,j-1/2}^{(l+1/2)} = \omega^l K e^{i\Sigma_t\lambda x_j} \ , \tag{12e}$$

$$\tilde{\Phi}_j^{(l+1)} = \omega^l I e^{i\Sigma_t\lambda x_j} \ , \tag{12f}$$

$$\tilde{\phi}_k^{(l+1)} = \omega^{l+1} E_r e^{i\Sigma_t\lambda x_j} \ . \tag{12g}$$

The quantities that are updated during inner iterations ($\tilde{\psi}_{k-1/2,n}^{(l+1/2,m)}$, $\tilde{\psi}_{k,n}^{(l+1/2,m)}$, and $\tilde{\phi}_k^{(l+1/2,m)}$) depend on the inner iteration variable m. We include this dependence in the Fourier ansatz by allowing

the coefficients $A_{r,n}^{(m)}$, $B_{r,n}^{(m)}$ and $F_r^{(m)}$ to vary during the high-order sweeps. The fine-grid error coefficients are also assumed to be periodic on the coarse grid, such that

$$\tilde{\psi}_{(k+p)-1/2,n}^{(l+1/2,m)} = \left(\tilde{\psi}_{k-1/2,n}^{(l+1/2,m)}\right) e^{i\Sigma_t\lambda\Delta} = \omega^l A_{r,n}^{(m)} e^{i\Sigma_t\lambda(x_j+\Delta)} \ . \tag{13}$$

Inserting the ansatz into Eqs. (9) and simplifying, we obtain:

$$F_r^{(0)} = E_r \ , \tag{14a}$$

$$\begin{cases} \frac{\mu_n}{h}\left(A_{r+1,n}^{(m)} - A_{r,n}^{(m)}\right) + \Sigma_t B_{r,n}^{(m)} = \frac{\Sigma_s}{2} F_r^{(m-1)} + \frac{\Sigma_a}{2} E_r \ , & 1 \le r < p \ , \\ \frac{\mu_n}{h}\left(A_{1,n}^{(m)} e^{i\Sigma_t\lambda\Delta} - A_{r,n}^{(m)}\right) + \Sigma_t B_{r,n}^{(m)} = \frac{\Sigma_s}{2} F_r^{(m-1)} + \frac{\Sigma_a}{2} E_r \ , & r = p \ , \end{cases} \tag{14b}$$

$$A_{1,n}^{(m)} = A_{1,n}^{(m)} e^{i\Sigma_t\lambda X} \ , \tag{14c}$$

$$\begin{cases} B_{r,n}^{(m)} = \left[\frac{1+\alpha_n}{2}\right] A_{r+1,n}^{(m)} + \left[\frac{1-\alpha_n}{2}\right] A_{r,n}^{(m)} \ , & 1 \le r < p \ , \\ B_{r,n}^{(m)} = \left[\frac{1+\alpha_n}{2}\right] A_{1,n}^{(m)} e^{i\Sigma_t\lambda\Delta} + \left[\frac{1-\alpha_n}{2}\right] A_{r,n}^{(m)} & r = p \ , \end{cases} \tag{14d}$$

$$F_r^{(m)} = \sum_{n=1}^{N} w_n B_{r,n}^{(m)} \ , \tag{14e}$$

$$D = \frac{1}{p}\sum_{r=1}^{p} F_r^{(M)} \ , \tag{14f}$$

$$2(I-D)(\cos(\Sigma_t\lambda\Delta) - 1) = 3\Sigma_t\Delta \sum_{n=1}^{N} w_n\mu_n A_{1,n}^{(M)}(e^{i\Sigma_t\lambda\Delta} - 1) \ , \tag{14g}$$

$$\sum_{n=1}^{N} w_n\mu_n A_{1,n}^{(M)} = e^{i\Sigma_t\lambda X} \sum_{n=1}^{N} w_n\mu_n A_{1,n}^{(M)} \ , \tag{14h}$$

$$0 = \sum_{j=1}^{J} e^{i\Sigma_t\lambda x_j} \ , \tag{14i}$$

$$\omega E_r - F_r^{(M)} = (I - D) \ . \tag{14j}$$

In Eqs. (14), we have used Eq. (9f) to rewrite the coarse-grid current error in terms of the edge-centered angular flux error. The resulting coarse-grid equations (Eqs. (14f) - (14j)) depend on the total number of inner iterations per outer (M), but do not depend explicitly on the inner iteration variable (m).

To proceed, we first use the periodic boundary condition Eq. (14c) to determine the permissible discrete Fourier frequencies:

$$\lambda = \lambda_s = \frac{2\pi s}{\Sigma_t X}, \quad s = 1, 2, 3 \ \ldots \ (J-1) \ . \tag{15}$$

These discrete frequencies depend on both the slab thickness (X) and number of coarse cells (J). When the discrete frequencies are applied to the Fourier ansatz, the normalization condition in Eq. (14i) is automatically satisfied.

Before a matrix system can be formed to solve for the theoretical spectral radius, we must express the scattering source error coefficients $F_r^{(M)}$ and coarse-grid current coefficient K in terms of the fission source error coefficients E_r. This process ultimately involves combining Eqs. (14g) and (14j) in vector form, and is omitted here due to page constraints (but will be included in a later publication). For the purposes of this paper, we assert that the scattering source flux and coarse-grid current error coefficients are related to the fission source flux error in the following way:

$$\mathbf{F}^{(M)} = \tilde{\mathbf{H}}^{(M)}\mathbf{E} \ , \tag{16}$$

$$K = \sum_{n=1}^{N} w_n \mu_n A_{1,n}^{(M)} = \sum_{r'=1}^{p} \tilde{A}_{1,r'}^{(M)} E_{r'} \ . \tag{17}$$

In Eq. (16), $\mathbf{F}^{(M)}$ is a size-p column vector containing the scattering source flux error coefficients $F_r^{(M)}$, $\mathbf{E}$ is a size-p column vector containing the fission source flux error coefficients E_r, and $\tilde{\mathbf{H}}^{(M)}$ is a $p \times p$ matrix which relates the two flux error vectors. In Eq. (17), $A_{1,n}^{(M)}$ are the edge-centered angular flux error coefficients for $r = 1$, and $\tilde{A}_{1,r'}^{(M)}$ are the quantities which relate $E_{r'}$ to the current error coefficient K.

Now that the scattering source flux and coarse-grid current error coefficients are expressed in terms of the fission source flux error coefficients, we proceed to the low-order equations. Substituting Eqs. (16) and (17) into Eqs. (14g) - (14j) (with the exception of the boundary and normalization conditions, which have already been satisfied), we obtain:

$$2(I - D)(\cos(\Sigma_t \lambda_s \Delta) - 1) = 3\Sigma_t \Delta \sum_{r'=1}^{p} \tilde{A}_{1,r'}^{(M)} E_{r'}(e^{i\Sigma_t \lambda_s \Delta} - 1) \ , \tag{18a}$$

$$\omega E_r - \sum_{r'=1}^{p} H_{r,r'}^{(M)} E_{r'} = (I - D) \ , \tag{18b}$$

where $\tilde{H}_{r,r'}^{(M)}$ are the components of $\tilde{\mathbf{H}}^{(M)}$ (see Eq. (16)). These two expressions can be combined to yield

$$2(\omega E_r - \sum_{r'=1}^{p} H_{r,r'}^{(M)} E_{r'})(\cos(\Sigma_t \lambda_s \Delta) - 1) = 3\Sigma_t \Delta \sum_{r'=1}^{p} \tilde{A}_{1,r'}^{(M)} E_{r'}(e^{i\Sigma_t \lambda_s \Delta} - 1) \ . \tag{19}$$

Moving all terms to one side of Eq. (19) and defining a lumped constant,

$$C = \frac{3\Sigma_t \Delta (e^{i\Sigma_t \lambda_s \Delta} - 1)}{2(\cos(\Sigma_t \lambda_s \Delta) - 1)} \ , \tag{20}$$

we arrive at the following eigenvalue system for ω:

$$C\sum_{r'=1}^{p}\tilde{A}_{1,r'}^{(M)}E_{r'}+\sum_{r'=1}^{p}H_{r,r'}^{(M)}E_{r'}-\omega E_r=0\ . \tag{21}$$

In matrix form, this can be expressed as

$$(\hat{\mathbf{H}}-\mathbf{I}\omega)\mathbf{E}=0\ , \tag{22}$$

where $\mathbf{I}$ is the $p\times p$ identity matrix, $\hat{\mathbf{H}}$ is a $p\times p$ matrix containing the coefficients of E_r from the first two terms of Eq. (21), and $\mathbf{E}$ is a size-p column vector which contains E_r.

Using Eq. (21), we calculate the eigenvalues ω_r numerically for $1\leq r\leq p$ and permitted values of the discrete Fourier frequency, λ_s. Once the eigenvalues are known, the spectral radius (ρ) is determined using

$$\rho=\sup_{1\leq s<J}\left[\sup_{1\leq r\leq p}|\omega_r(\lambda_s)|\right]. \tag{23}$$

5 NUMERICAL RESULTS

The test problem considered in this paper is a homogeneous 1000-centimeter (cm) slab with periodic boundaries. Numerical problem data are provided in Table I. The total cross section, fission cross section, and fine grid size are fixed for all cases, while the scattering ratio, coarse grid size, and number of inner iterations per outer are allowed to vary. We require that the coarse-grid parameter (p) be an integer, and we also require an integer number of coarse cells in the 1000-cm slab. All cases were run with the S_8 Gauss-Legendre quadrature set.

Table I. Test Problem Specifications

Σ_t (cm^{-1})	$\nu\Sigma_f$ (cm^{-1})	h (cm)	Σ_s (cm^{-1})	M (#)	Δ (cm)
1.0	0.01	0.2	0.0 - 0.99	1, 2, 3, 5, 10, 20	1, 1.6, 2, 4, 8, 10, 20

To assess the validity of the Fourier analysis, we compare our theoretical results to numerical estimates from direct simulations. Our S_N-CMFD simulations use vacuum boundary conditions. While the numerical test problem could in theory be run with periodic boundaries, it is not guaranteed that the boundary conditions will be satisfied if the number of inner iterations per outer (M) is small. (The linearization procedure outlined in Section 3 requires that the exact solution of the theoretical problem be flat, which precludes the possibility of Fourier-analyzing the vacuum boundary case.) To address this issue, we implemented a modified iteration scheme that allows the periodic boundary condition to converge while only updating the scattering source a fixed number of times. Numerical results from the modified periodic boundary simulations agree closely with the vacuum boundary results presented here.

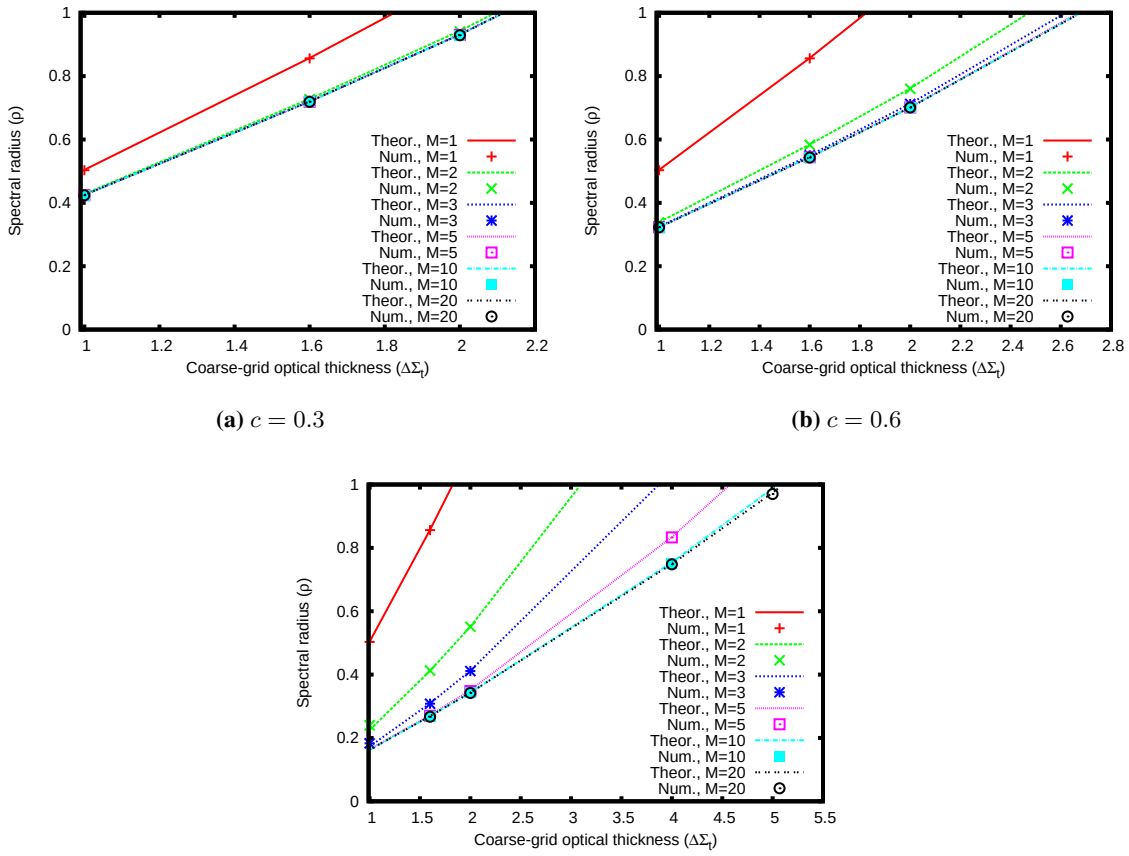

(a) $c = 0.3$

(b) $c = 0.6$

(c) $c = 0.9$

Figure 1. Spectral radius (ρ) vs. coarse-grid optical thickness for different values of c

The plots in Fig. 1 compare the numerical spectral radius estimates to theoretical predictions for $c = 0.3$, 0.6 and 0.9. We observe close agreement between the theoretical and numerical values for all cases. For all three values of the scattering ratio c, the theoretical curves approach the implicit-scattering limit as M increases [9], and effectively overlap for $M \geq 10$.

In particular, all three plots in Fig. 1 show excellent agreement for the special case of $M = 1$ (a single inner iteration per outer). Predictions from our Fourier analysis indicate that the $M = 1$ spectral radius should be independent of the scattering ratio, c. Indeed, the $M = 1$ numerical spectral radii are independent of the scattering ratio, and depend only on the coarse grid optical thickness.

Using linear interpolation between theoretical data points, we generated constant-spectral-radius curves for $M = 2,\ 3,\ 5$ and 10. These curves are plotted in Fig. 2 as a function of the coarse-grid optical thickness $\Sigma_t\Delta$ and scattering ratio c. They show that as M (the number of inner iterations per outer) increases, the spectral radius (ρ) decreases. The iteration scheme is stable for the phase space to the left of the pink $\rho = 1$ curve, and unstable for the phase space to the right of this curve.

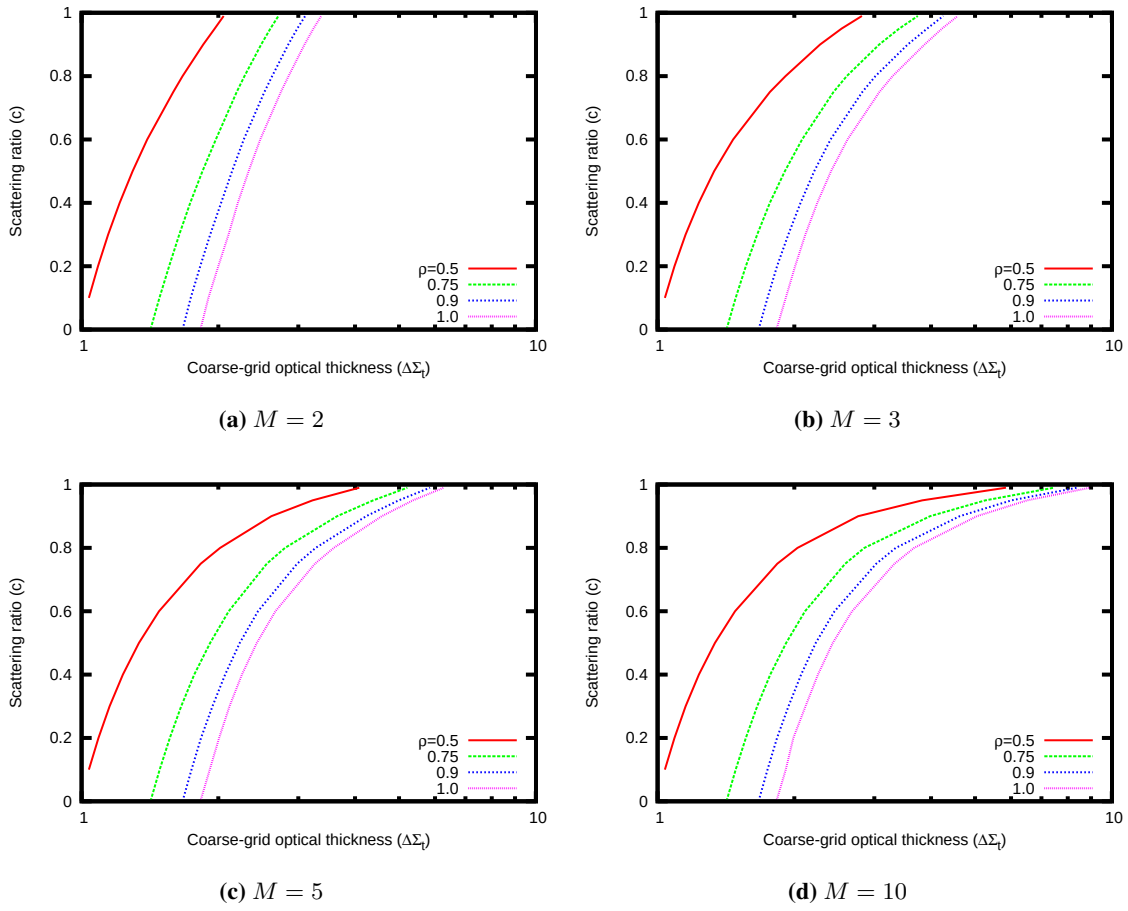

(a) $M = 2$ **(b)** $M = 3$

(c) $M = 5$ **(d)** $M = 10$

Figure 2. Constant-ρ curves for different values of M

When the scattering ratio c is small, the constant-rho curves depend only mildly on the number of inner iterations per outer (M). This means that a simulation run with a small value of M will converge at roughly the same rate as a simulation with a large value of M. For more highly scattering problems ($c \sim 0.9$ or greater), the constant-ρ curves shift significantly to the right with increasing M until $M \approx 10$. In this regime, simulations that are stable when M is large may become unstable if M is reduced to a small value. Conversely, simulations that are unstable with a small value of M may become stable if M is increased.

All four sets of curves in Fig. 2 depict monotonically-increasing functions of the scattering ratio; as c increases, the coarse-grid size corresponding to a fixed value of ρ also increases. In other words, the S_N-CMFD stable grid size limit increases as the scattering ratio increases. This implies that the S_N-CMFD method converges more rapidly as the scattering ratio of the problem increases for a fixed grid size.

For the special case of $c = 0.0$ (purely-absorbing), the spectral radius is independent of the number of high-order inner iterations performed. In the absence of scattering, the S_N-CMFD method becomes unstable when the coarse grid is slightly less than 2 mfp thick (for the 0.2 mfp fine

grid considered here). As $c \to 1.0$ (purely-scattering), the stable grid size tends to infinity.

6 CONCLUSIONS

In this work, we present a Fourier analysis of the S_N-CMFD method for *k*-eigenvalue problems. The problem considered here is isotropic and monoenergetic; however, our Fourier analysis could be extended to treat problems with anisotropic scattering, as well as multigroup energy dependence. The same general procedure could also be used to Fourier-analyze a variety of differencing schemes for both the high- and low-order equations. We consider the S_N-CMFD method primarily because the results are applicable to our research in hybrid Monte Carlo-CMFD methods [9].

The S_N-CMFD iteration scheme includes the following steps: (i) perform a specified number of sweeps to obtain an updated scattering source flux, (ii) calculate the coefficients of the coarse-grid system, (iii) solve the low-order system to obtain an updated coarse-grid fission source, and (iv) use this coarse-grid fission source estimate to scale the fine-grid fission source for the next cycle.

Because the S_N-CMFD iteration scheme is nonlinear, we linearize the S_N-CMFD equations for a problem with periodic boundary conditions, and then Fourier-analyze the linearized equations. The result of this analysis is a matrix system that is solved numerically for the theoretical spectral radius.

To assess the validity of the Fourier analysis, we compare theoretical predictions to estimates from direct numerical simulations. The numerical estimates are generated for a large slab problem with vacuum boundaries. Despite slight leakage effects in our numerical simulations, the theoretical and numerical values agree well for all cases.

The Fourier analysis correctly predicts a number of trends in the S_N-CMFD spectral radius. Specifically, the spectral radius (i) increases as the coarse-grid optical thickness increases, (ii) decreases as the scattering ratio increases (with the exception of the $M = 1$ case discussed previously), and (iii) decreases as the number of inner iterations per outer increases.

These trends indicate that an unstable S_N-CMFD simulation can likely be made stable by reducing the coarse grid size or increasing the number of inner iterations per outer (or both). It is the hope of the authors that these theoretical insights will help guide code users in selecting stable parameters for practical simulations.

7 ACKNOWLEDGMENTS

We gratefully acknowledge support from the Consortium for Advanced Simulation of Light Water Reactors (www.casl.gov), an Energy Innovation Hub (http://www.energy.gov/hubs) for Modeling and Simulation of Nuclear Reactors under U.S. Department of Energy Contract No. DE-AC05-00OR22725.

8 REFERENCES

[1] J. Yoon and H. Joo, "Two-Level Coarse Mesh Finite Difference Formulation with Multigroup Source Expansion Nodal Kernels," *Prog. Nucl. Energy*, **45**, pp. 668–682 (2002).

[2] Z. Zhong, T. Downar, Y. Xu, M. DeHart, and K. Clarno, "Implementation of Two-Level Coarse-Mesh Finite Difference Formulation in an Arbitrary Geometry, Two-Dimensional Discrete ordinates Transport Method," *Nucl. Sci. Eng.*, **158**, pp. 289–298 (2008).

[3] K. Moon, N. Cho, J. Noh, and S. Hong, "Acceleration of the Analytic Function Expansion Nodal Method by Two-Factor Two-Node Nonlinear Iteration," *Nucl. Sci. Eng.*, **132**, pp. 194–202 (1999).

[4] M. Adams and E. Larsen, "Fast Iterative Methods for Discrete-Ordinates Particle Transport Calculations," *Prog. Nucl. Energy*, **40**, pp. 3 (2002).

[5] K. Smith and J. Rhodes, "Full-Core, 2-D, LWR Core Calculations with CASMO-4E," *Proc. PHYSOR 2002*, Seoul, Korea, October 7-10, 2002, 2002.

[6] E. Larsen and B. Kelley, "The Relationship Between the Coarse-Mesh Finite Difference and the Coarse-Mesh Diffusion Synthetic Acceleration Methods," *Nucl. Sci. Eng.*, **178**, pp. 1 (2014).

[7] D. Lee, T. Downar, and Y. Kim, "Convergence Analysis of the Nonlinear Coarse-Mesh Finite Difference Method for One-Dimensional Fixed-Source Neutron Diffusion Problem," *Nucl. Sci. Eng.*, **147**, pp. 127 (2004).

[8] S. Hong, K.-S. Kim, and J. Song, "Fourier Convergence Analysis of the Rebalance Methods for Discrete Ordinates Transport Equations in Eigenvalue Problems," *Nucl. Sci. Eng.*, **164**, pp. 33 (2010).

[9] K. Keady and E. Larsen, "Stability of Monte Carlo k-Eigenvalue Simulations with CMFD Feedback," *J. Comp. Phys.* (Submitted Nov 2014).